Online Estimation of Cable Harmonic Impedance in Low-Voltage Distribution Systems

Stanislav Babaev, Sjef Cobben, Vladimir Ćuk, and Helko van den Brom, *Senior Member, IEEE*

***Abstract*— Incorrect values of cable harmonic impedance can lead to wrong conclusions when assessing an impact of current distortion on the power network. A theoretical derivation of resistance and reactance for harmonic frequencies is not sufficient as it neglects operating conditions of cables as well as their configuration and actual installation pattern. In this paper, a noninvasive procedure for estimating parameters of the low-voltage cable is proposed. On contrary to invasive methods, the proposed technique does not require any external sources of harmonic excitation, and consequently, it does not introduce additional disturbances to the system. A disconnection of the cable is not required as the procedure meant to be performed online. The methodology employs natural variations of harmonic currents and voltages; however, the impedance angle is preserved due to the utilization of synchronized measurement samples. The developed signal processing algorithm provides noise reduction capabilities and smoothing of the output in presence of fluctuating harmonics. In addition, an attention is given to the metrological characterization of the measurement system and evaluation of uncertainty of impedance values. The results of the laboratory experiment indicate that for selective harmonics the variations of impedance estimates are no more than 10 mΩ, which is in the range of calculated uncertainty values. The practical applicability of the method is discussed together with its limitations.**

***Index Terms*— Impedance measurement, measurement techniques, measurement uncertainty, power quality, power system harmonics.**

I. Introduction

THE harmonic impedance of cables and transmission lines plays a critical role in harmonic analysis. Accurate impedances at all frequencies of interest are necessary for evaluation of harmonic emission levels, identification of potential resonance problems and design of adequate mitigation measures. It is known that cable impedance under nonsinusoidal conditions can deviate significantly from theoretical values derived from 50-Hz resistance and reactance. The analytical expressions and finite element methods presented in the current literature demonstrate that it is the proximity effect which is responsible for unique harmonic behavior of cables. As Chien and Bucknall [1] pointed out in their investigation on subsea power transmission cable, the proximity effect in multi-conductor cables leads to a drastic increase in both resistance and reactance with raising frequencies. The results of this paper were confirmed in [2], with additional regard to the asymmetrical distribution of eddy currents in a three-core submarine cable.

Fundamentally, the harmonic behavior of the subsea cables is different from underground ones. Urquhart and Thomson [3] provided a thorough survey on the existing modeling strategies of underground low-voltage distribution cables. It was proven that sufficient discrepancies in results can occur at harmonic frequencies when employing models with different complexity levels. Moreover, another important observation concerned the impact of the ground path on zero-sequence resistance, which can be altered sufficiently depending on the grounding strategy. Furthermore, the measurements performed on the disconnected low-voltage cables by utilization of an external signal generator revealed the additional impact of cable configuration and installation practice on final harmonic impedance values [4], [5]. In addition, a steel wire armor has been accounted for being responsible for the extra increase in cable resistance due to eddy current losses.

If cable design data are available, it is possible to obtain estimates of impedance through the application of the aforementioned modeling techniques. However, in many cases, these data are difficult to acquire, and approximation of impedance values remains uncertain. Therefore, accurate measurements of resistance and reactance at different frequencies are required. Moreover, in order to take into account all the deciding factors including cable laying, its configuration, neutral grounding strategy and asymmetry in harmonic current injections, the impedance measurement should be performed on-site on already installed cables.

Several papers address the issue of determining parameters of lines at fundamental frequency without putting them out of service. The most recent state-of-the-art focuses on state estimation techniques involving synchronized phasor data. Among others are contributions [6]–[9] which presented the methodology for estimating line parameters for high-voltage transmission systems with provision of phasor measurement units (PMUs). Furthermore, a method applicable to distribution system level was proposed in [10]. In this paper, the authors determined the parameters of medium-voltage

Manuscript received February 14, 2019; revised June 17, 2019; accepted June 22, 2019. Date of publication July 3, 2019; date of current version May 12, 2020. This work was supported by the European Union's Horizon 2020 Research and Innovation Program (MEAN4SG) through the Marie Skłodowska-Curie Grant under Contract 676042. The Associate Editor coordinating the review process was Daniele Fontanelli. *(Corresponding author: Stanislav Babaev).*

S. Babaev, S. Cobben, and V. Ćuk are with the Department of Electrical Engineering, Eindhoven University of Technology, 5612 AZ Eindhoven, The Netherlands (e-mail: s.babaev@tue.nl).

H. van den Brom is with the Dutch Metrology Institute (VSL), 2629 JA Delft, The Netherlands (e-mail: hvdbrom@vsl.nl).

Color versions of one or more of the figures in this article are available online at http://ieeexplore.ieee.org.

Digital Object Identifier 10.1109/TIM.2019.2926690

feeders considering uncertainties associated with transducer errors. On the other hand, little attention has been paid in the literature to online impedance characterization of underground cables of low-voltage distribution systems.

In this paper, a novel method for estimating impedance of the low-voltage cable is proposed. The method aims to resolve resistance and reactance values at different frequencies in the presence of fluctuating harmonics in the system. An additional source of harmonic excitation is not required, neither the disconnection of loaded cable. The proposed method is based on the utilization of natural harmonic current and voltage variations of nonlinear loads. These signals are captured synchronously at multiple points by a measurement system with high accuracy level. The impedance is then estimated in the form of transfer function preserving phase angle values. The indicative uncertainty values associated with the measurement chain allow rejecting unreliable input data and establishing confidence interval for final impedance values.

II. Methodology

A. Laboratory Setup

The online estimation of cable harmonic impedance value was performed in the laboratory. The established power network infrastructure includes a low-voltage power source and underground low-voltage 70 mm^2 Al feeder with an approximate length of 150 m. Overall, there are six connection points along the cable realized with 16 mm^2 Cu of 30 m length each. These connections act as conventional "households" and different types of loads can be connected thereto. Thus, this configuration represents a part of a typical low-voltage network in the urban environment. It is worth noting that combined dc resistance of the main feeder together with the last section of household connection was measured with the external dc source. For this purpose, two identical digital multimeters Agilent 34401A were installed at the beginning of the feeder and at the last connection point to measure the value of the voltage drop across the dc resistance. These multimeters are characterized by 0.0030% gain error and 0.0005% offset error as per data provided by the manufacturer. The dc source provided controlled excitation from 1 to 10 A and current measurements with calibrated accuracy 0.5% + 2 digits. The dc current was drawn by precision current measurement shunts with calibrated resistances of 10 and 100 mΩ which were connected to the last household. The measurements were repeated 13 times for different current levels, and after each subsequent step new value of resistance was calculated. The majority of results was included between boundaries of 0.0934 and 0.0936 Ω. Based on this, the value of 0.0935 Ω is taken as the reference. Furthermore, the reactance at fundamental frequency was calculated based on the layout and data sheet specifications. The value of 0.023 Ω is accepted as reference reactance. The proposed experiment involves the use of a nonlinear programmable load California Instruments 3091LD which acts as an emulator of real large power electronics-based load. This load provides harmonic current injections which are used as an input for methodology described in this paper. Furthermore, two identical solar inverters

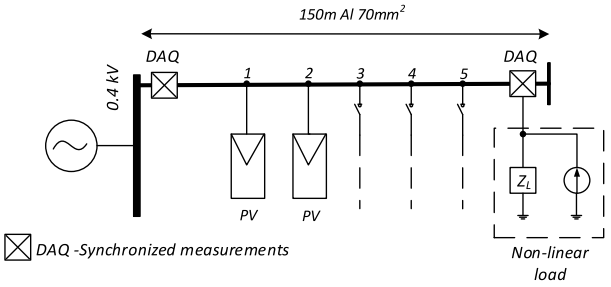

Fig. 1. Experimental setup.

Mastervolt Soladin 3000 Web are connected toward the beginning of the feeder. These inverters are supplied by Solar Power Simulator TerrasSAS ETS, which can emulate the operation of the solar power plant under different irradiation levels. The purpose of the inverters is to provide small current distortions and, therefore, to act as a source of additional noise in the system. These solar inverters operate with rated total harmonic distortion (THD) level less than 3%, therefore ensuring the only little impact on harmonic voltage drop. Furthermore, both public low-voltage grid and programmable voltage source California Instruments MX45 are used during the experiment. The one-line configuration of the setup with measurement points is depicted in Fig. 1. More details about the measurement system are provided below.

B. Measurement System

Distributed high-accuracy fast data acquisition system consists of two National Instruments cRIO-9038 chassis. Voltage and current waveforms are recorded at 25 kHz sampling frequency with all the samples synchronized across all channels and chassis to the precision time source. The clock signal is generated on field-programmable gate array (FPGA) of the master device and then distributed via a high-speed digital interface to the slave device. The digital modules used for this procedure are NI-9401. Thus, both of the acquisition devices are triggered synchronously at the start of the data recording. The accuracy of time synchronization is at the range of 200 ns.

Voltage signals are measured directly at both ends of the cable whereas line current is provided by Rogowsky coil type PEM LFR 03/3. The chassis is equipped with input voltage NI-9225 and current NI-9234 measurement cards with 24-bits analog-to-digital converters (ADC) based on delta-sigma technology. This implies that the output of ADC is characterized by the unequal amount of samples produced from one cycle to another. Thus, a resampling algorithm is utilized as a part of the developed synchronization software package. Furthermore, the voltage cards contain three differential input channels with channel-to-channel isolation excluding the possibility of ground loop influence. In contrast, all four input channels of current measurement cards are referenced to the chassis ground through a resistor. Thus, in order to avoid the possible impact of ground loops all the chassis were connected to the common ground. For the correct performance of the proposed methodology, only single-phase current and additionally neutral conductor current are sufficient

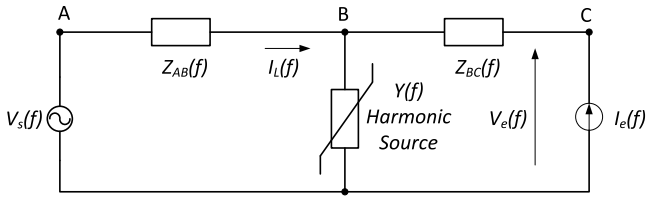

Fig. 2. Equivalent circuit.

to measure. These measurements are placed at the beginning of the cable involving, therefore, only two input channels out of available four.

The recorded data were stored directly on the hard drive of each measurement device, therefore eliminating all potential delays associated with the transfer of data via Ethernet or other means of communication.

C. Fundamental Idea

The fundamental idea behind the calculation of cable harmonic impedance is the utilization of natural excitation of the system provided by the operation of nonlinear loads. Thus, the following equation is sufficient:

$$Z(f) = \frac{V_1(f) - V_2(f)}{I(f)} \tag{1}$$

where $V_1(f)$ and $V_2(f)$ are the voltages measured at the beginning and end of the cable, respectively, and $I(f)$ is a line current measured at the sending end of the cable. For low-voltage systems, it is reasonable to assume that the current difference between sending and receiving end of the cable is negligible. It is evident from (1) that, for correct calculation of the line harmonic voltage drop and subsequently estimation of the impedance, all the values must be recorded synchronously. Some considerations on this problem were reported in [11].

The cable impedance can be estimated within a certain degree of accuracy when particular nonlinear load provides sufficient harmonic excitation levels. These harmonic currents, in turn, cause line voltage drop at different frequencies. As it will be pointed out later, an efficient noise-reducing algorithm is crucial for the successful performance of the proposed method. In addition, an important consideration is in order: the impedance is estimated up to the point of connection of dominant harmonic producing source, i.e., for obtaining the value which corresponds to the full length of the cable, the load must be connected at the end of it. This idea is illustrated in Fig. 2, where a dominant harmonic source represented by complex admittance $Y(f)$ is connected to point B after the impedance section $Z_{\mathrm{AB}}(f)$. Given the source voltage $V_s(f)$ and voltage at the end of the cable $V_e(f)$, the goal of the proposed methodology is to estimate the value of $Z_{\mathrm{AB}}(f)$ over which the harmonic voltage drop occurred during the operation of dominant harmonic load $Y(f)$. At the same time, the critical part is to filter out the uncorrelated noise and impact of another harmonic producing loads $I_e(f)$. Furthermore, the proposed method makes use of single-phase measurement. Additional neutral-wire measurements are employed for unbalanced situations and compensation of zero-sequence harmonics.

D. Estimation Algorithm

One of the main issues for accurate estimation of harmonic impedance with noninvasive methods is voltage background harmonics. These background harmonic components introduce an error in the final estimated value of the impedance. Due to the fast dynamic nature of background distortion, the elimination of their impact is a nontrivial task. When the harmonic impedance of the cable is of concern, another origin of the error is the combined effect of simultaneous operation of all the other loads connected along the feeder. The level of excitation provided by these loads can be quite low, yet reasonable enough to act as a source of the noise.

Taking into account the aforementioned, Babaev *et al.* [12] demonstrated the challenge of employing just a few cycles of rms values (magnitudes only) for impedance calculation, as these values have to be chosen from certain strict realizations of data. A considerable improvement is to perform a continuous assessment of the impedance over the range of frequencies by utilizing a large amount of data samples. The underlying signal processing algorithm proposed in this paper is referred to Welch Averaged Periodogram. Generally, the periodogram is an efficient way to provide an estimator for the power spectrum. The basic concept of periodogram calculation is to establish the correlation estimate of the signal and after that apply Fourier transform. Thus, both pure windowed sequences of a signal and its shifted version are used in the estimation procedure. The following equation (2) sets the correlation sequence:

$$c_{\mathrm{vv}}[m] = \sum_{n=0}^{L-1} x[n]w[n]x[n+m]w[n+m] \tag{2}$$

where L is a length of the signal, $x[n]$ is a given signal and $w[n]$ is a window sequence.

The fundamental property of the periodogram estimate is the increasing variance with the frequency when the length of the window m approaches the signal length L. On the other hand, obtaining smooth estimate of the power spectrum requires decreasing the length of the signal and number of DFT points, which leads to poor frequency resolution. For considering this tradeoff, Welch [13] suggested to reduce random variations of the estimate by breaking the signal into several independent periodograms and then averaging their output. The equation (3) for autocorrelated power spectrum, therefore, can be written as follows:

$$P_{\mathrm{xx}}(\omega) = \sum_{-\infty}^{\infty} c_{\mathrm{vv}}[m]e^{-j\omega m} \tag{3}$$

This type of signal processing algorithm is best suitable for working with noisy signals, for any uncorrelated noise can be removed from the system. At the same time, the important features of the input and output are conveniently represented by averages.

In order to apply the described algorithm for harmonic impedance estimation the notion of Linear Time Invariant (LTI) system is used. The attributes of that system are such that it is fully described by its impulse response. This impulse response, in turn, can be utilized to calculate the output of

the system due to any input occurred. The following general equation (4) is applied:

$$y[n] = x[n]h[n] \tag{4}$$

where $y[n]$ is the output of the system, $x[n]$ is the input, and $h[n]$ is the impulse response. Furthermore, the concept of LTI system implies that output $y[n]$ is expressed by means of all the samples of impulse response and input sequences, which are linearly superimposed and shifted accordingly in time. This feature provides a foundation for continuous assessment of harmonic impedance [14]. The impulse response $h(\omega)$ is then can be estimated as

$$h(\omega) = \frac{P_{\mathrm{xy}}(\omega)}{P_{\mathrm{xx}}(\omega)} \tag{5}$$

where $P_{\mathrm{xy}}(\omega)$ is cross-correlated power spectrum of line voltage drop and line current and $P_{\mathrm{xx}}(\omega)$ is autocorrelated power spectrum of current. The output of (5) is equivalent to the impedance values calculated at different frequencies.

It is worth noting that all fast Fourier transform (FFT)-based algorithms are prone to the issue of spectral leakage in case of the systematic deviation of power frequency in the system. In order to address this problem, the parameters of the Welch averaged periodogram were tuned according to the following logic.

1) The cable under the study and one nonlinear load were energized by the external power source providing stable sinusoidal voltage with constant frequency of 50 Hz.
2) The resistance and reactance values were extracted for selective frequencies by applying proposed algorithm.
3) The same steps were performed after substituting the external power source with a public grid which is characterized by deviating power frequency.
4) The parameters of the algorithm were established by analyzing differences in impedance results between the ideal case with fixed frequency and public grid connection.

Based on 25-kHz sampling frequency, the one-cycle Hamming window and 500 DFT points were used. Moreover, 10-s segments of a signal were further broken into 500 independent periodogram with 10% overlap. Consequently, the impact of the spectral leakage was reduced and smooth averaged output was obtained. However, in order to completely eliminate this phenomenon the window of the FFT has to be synchronized to the actual power frequency. This technique nevertheless was out of the scope of the presented experiments. The block diagram of the proposed algorithm is shown in Fig. 3.

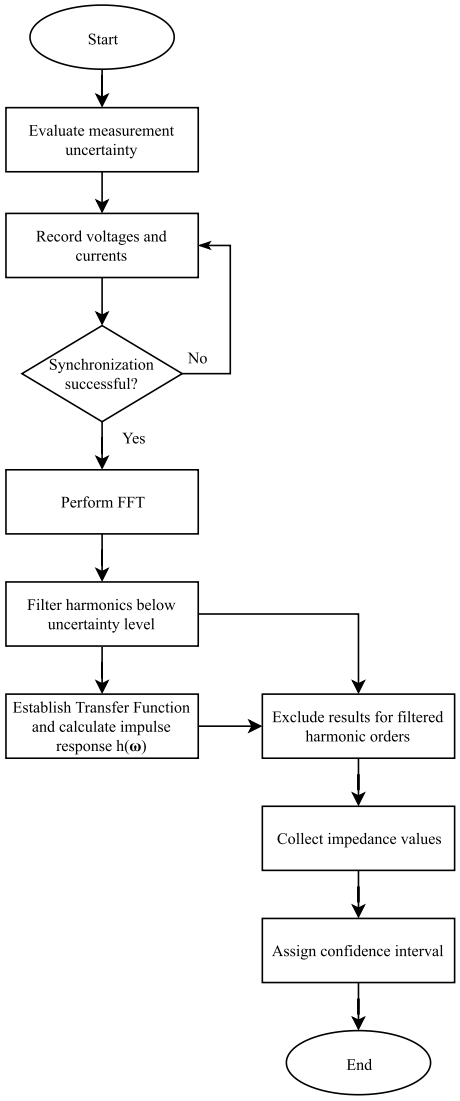

Fig. 3. Flowchart of the proposed algorithm.

III. Evaluation of Measurement Uncertainty

The evaluation of uncertainty in this paper is based on the metrological specifications of measurement equipment. Therefore, Type B uncertainty is calculated according to Guide to the Expression of Uncertainty in Measurement [15] recommendations. The typical calibration values for each component of the measurement chain are given in Table I. The antialias bandwidth of voltage and current cards is 22 kHz and reported values for current probes are valid for frequency range from 0.45 to 20 kHz.

TABLE I
Equipment Specifications

Component	Gain error, %	Offset error, %	Noise, mV
Voltage card	±0.05	±0.008	2
Current card	±0.05	±0.006	0.05
Current probe	±0.3	±0.05	3

First, a standard uncertainty associated with each component of voltage and current measurements is evaluated. Furthermore, a combined standard uncertainty for current is computed through application of summation in quadrature

$$u_c(I) = \sqrt{u_1(I)^2 + u_2(I)^2} \tag{6}$$

where $u_1(I)$ and $u_2(I)$ are the standard uncertainties of input current card and current probe, respectively.

Finally, the uncertainty of the impedance estimation involves correlated input quantities. The degree of correlation

TABLE II
UNCERTAINTY BUDGET

Quantity	Standard uncertainty $u(x_i)$	Probability	Expanded uncertainty k factor = 2
Minimum excitation, I = 9.05 A			
V	70 mV	normal	140 mV
I	2.9 mV	normal	5.8 mV
Z	7.7 $m\Omega$	normal	15.4 $m\Omega$
Medium excitation, I = 10.84 A			
V	70 mV	normal	140 mV
I	3.3 mV	normal	6.6 mV
Z	5.9 $m\Omega$	normal	11.8 $m\Omega$
Maximum excitation, I = 13.38 A			
V	70 mV	normal	140 mV
I	3.6 mV	normal	7.2 mV
Z	5.2 $m\Omega$	normal	10.4 $m\Omega$

is estimated through correlation coefficient according to

$$r(V, I) = \frac{u_c(I)\delta_V}{u_c(V)\delta_I} \tag{7}$$

where $u_c(I)$ and $u_c(V)$ are combined standard uncertainties of current and voltage measurements, respectively, and δ_I and δ_V are current perturbation and associated voltage drop, respectively. The combined standard uncertainty for correlated input quantities is given as

$$u_c(Z) = c_V^2 u_c^2(V) + c_I^2 u_c^2(I) + 2u_c(V)u_c(I)r(V, I)c_V c_I \tag{8}$$

where c_V and c_I are the sensitivity coefficients. The sensitivity coefficients are calculated as follows

$$c_V = \frac{\partial Z}{\partial V} \tag{9}$$

$$c_I = \frac{\partial Z}{\partial I}. \tag{10}$$

Several remarks should be given with respect to evaluated combined uncertainty of impedance magnitude. The correlation coefficient in (7) is frequency dependent and, therefore, its value will be increasing with increased frequency due to higher value of impedance. Furthermore, the second term of (8) takes the negative sign and, thus, the final uncertainty is expected to decrease with higher order of harmonics, provided that voltage and current readings are above the uncertainty level of the measurement system. The estimated uncertainty budget for fundamental frequency is presented in Table II.

IV. RESULTS

A. Programmable Voltage Source

During this experimental case only three-phase balanced nonlinear load was connected to the household #6 which corresponds to the connection point at the end of the cable. The load with maximum apparent power of 3 kVA per phase was programed to operate as constant power load with crest factor 1.8. This provided sufficient excitation level for the positive-sequence and zero-sequence harmonics. The programmable power source with fixed fundamental frequency of 50 Hz and low level of voltage waveform distortion was used to supply the load. Several excitation levels have been tested and some of the loading scenarios are presented in Table III.

TABLE III
LOAD OPERATING SCENARIOS [1]

#	1	2	3	4	5	6	7	8	9
I_1, A	13.0	10.8	11.7	12.8	11.3	12.6	13.0	9.0	13.9
P_1, kW	2.9	2.5	2.6	2.9	2.6	2.9	3.0	2.0	3.0

[1] constant power load with crest factor of 1.8

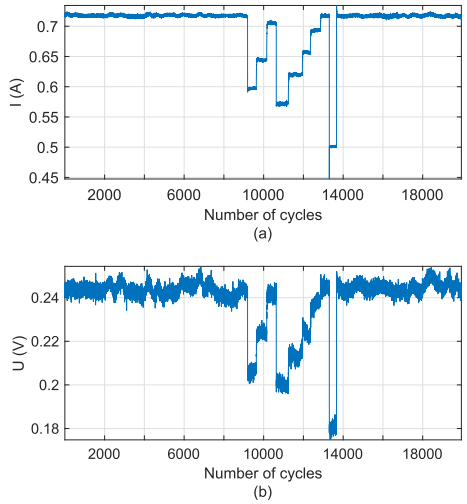

Fig. 4. Seventh-harmonic one-cycle rms values. (a) Load current. (b) Voltage at the beginning of cable.

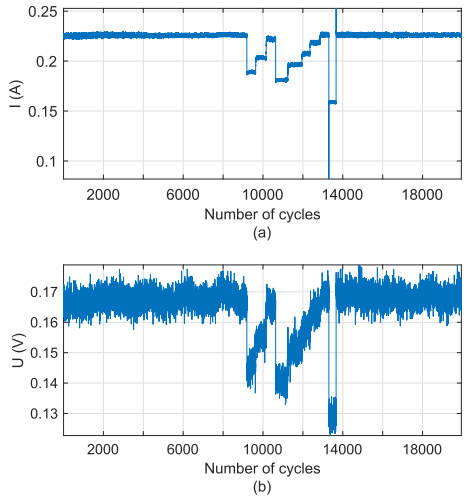

Fig. 5. Thirteenth-harmonic one-cycle rms values. (a) Load current. (b) Voltage at the beginning of cable.

As an example, Figs. 4 and 5 show pattern of the harmonic load current together with associated voltage distortion at the sending end of a cable for 7th and 13th harmonic orders, respectively. The overshoots are due to imperfections in the control of load bank during rapid change of load demand.

It follows from the detailed analysis of these graphs that lower harmonic current value at higher harmonic orders contributes to a larger voltage distortion due to increased

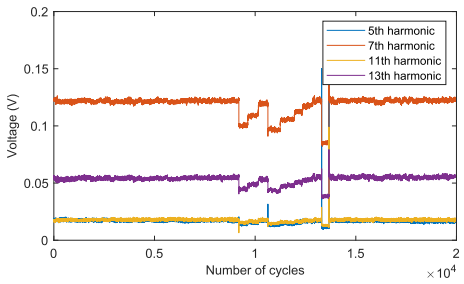

Fig. 6. Voltage drop at different frequencies.

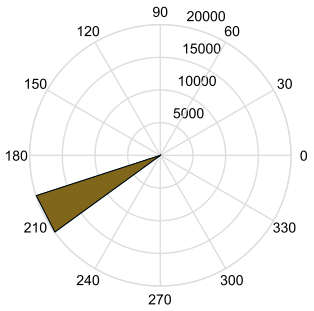

Fig. 7. Angle between ΔV and I at the seventh harmonic.

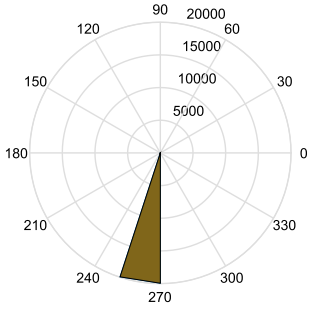

Fig. 8. Angle between ΔV and I at the eleventh harmonic.

value of the impedance. This is followed by significantly larger magnitude variations of harmonic voltage when frequency increases. To conclude this qualitative analysis, a graph demonstrating cable voltage drops at different harmonic frequencies is presented in Fig. 6. The recorded voltage drop values for 5th and 11th harmonics are significantly smaller than corresponding values of 7th and 11th and almost close to the uncertainty level of voltage acquisition cards. Therefore, the uncertain harmonics must be excluded from impedance estimation algorithm. Furthermore, it is important to carefully consider excitation levels for both resistive and reactive parts. This requires evaluation of angle between voltage drop ΔV over the cable and corresponding load current I at frequencies of interest. Histogram angle charts of relative angle values are shown in Figs. 7 and 8 for 7th- and 11th-harmonic orders, respectively. For 11th harmonic, it indicates that voltage drop is caused exclusively by imaginary component and taking into consideration small magnitude of ΔV it is reasonable to infer that calculation of resistive part of cable impedance will give erroneous result.

It is worth noting that a three-phase balanced nonlinear load can inject zero-sequence harmonics which tend to add in

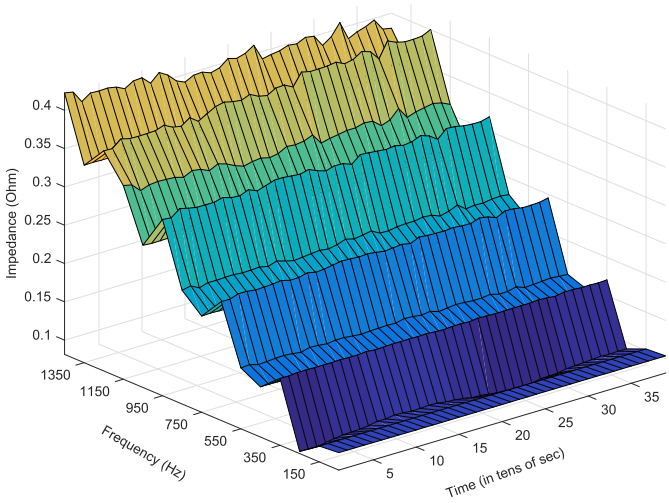

Fig. 9. Magnitudes of cable impedance values at different frequencies

TABLE IV
COMPLEX IMPEDANCE VALUES

h #	$R+iX$ Ω	$\mid Z \mid$ Ω	Standard uncertainty $m\Omega$	I A
1	0.1037 + 0.0097i	0.1042	7.7	9.05
3	0.0953 + 0.0363i	0.1020	3.8	3.93
7	0.1478 + 0.0814i	0.1687	25.5	0.5
9	0.0982 + 0.1092i	0.1469	62.1	0.25
13	0.1894 + 0.1417i	0.2365	82.3	0.16
15	0.1050 + 0.1783i	0.2069	442.4	0.04
19	0.2418 + 0.1964i	0.3115	274.5	0.06

neutral wire and thus create an uneven voltage drop over zero-sequence impedance. In theory, these triple components are expected to be exactly three times of the corresponding phase value. However, in practical situation, due to the leakage effect to the ground the magnitude of current in neutral wire can demonstrate some deviations from anticipated value. In order to complement the proposed method and avoid employment of three phase measurements and corresponding complexity of constructing three phase equations involving mutual coupling phenomena, it is suggested to use neutral wire measurement for compensation of triple components.

By employing the algorithm described in Section II, the impedance values of a cable were calculated and results are presented in Fig. 9. It is worth of noting that harmonic values for even orders were excluded from calculation due to low-excitation levels and, therefore, are not presented in the graph. The analysis of results reveals that proposed algorithm provides sufficient noise reducing capabilities and gives stable estimates of impedance over the course of time.

Furthermore, the performance of the method proved to be robust during dynamic test, i.e., alteration of load demand in fast steps. The estimated impedances for harmonic orders from 1 to 19 along with standard uncertainties and harmonic current values are presented in Table IV. From this table, it can be inferred that the magnitude of the estimated fundamental impedance is close to the accepted reference value of 0.0963 Ω. The difference between two values

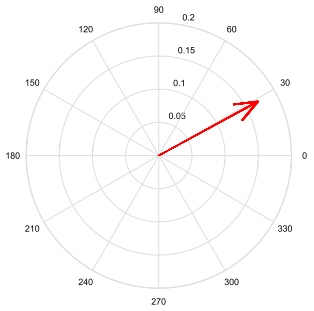

Fig. 10. Seventh-harmonic impedance.

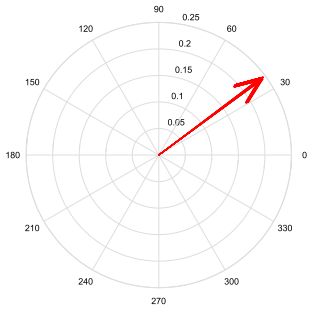

Fig. 11. Thirteenth-harmonic impedance.

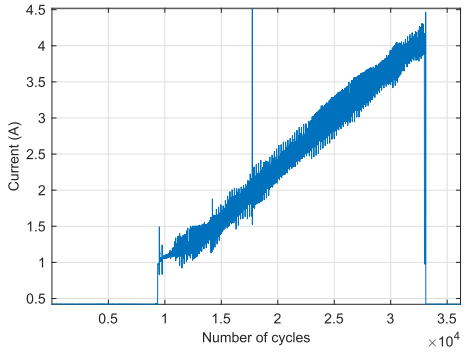

Fig. 12. Inverter fundamental output current.

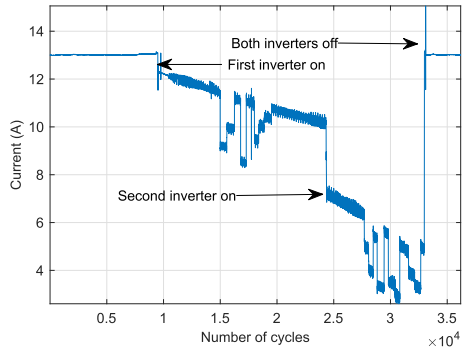

Fig. 13. Fundamental line current.

is 7.9 mΩ, which is within the evaluated expanded uncertainty for this frequency for 95% of values (coverage factor k = 2). The main difference lies in the reactive part of impedance and this is due to the initially low X/R ratio which requires higher excitation levels in imaginary part of current.

Furthermore, the highest harmonic current of 3.93 A was recorded for third-harmonic component which also corresponds to the lowest standard uncertainty of 3.8 mΩ. This is governed by the fact that, at this frequency, harmonic current had the largest impact on the voltage. In addition, due to the increased correlation via higher impedance the uncertainty level decreased. Furthermore, the harmonic impedance estimates demonstrate consistent increasing behavior. It is worth of noting that reactive part changes closely to widely accepted theoretical formulation. Moreover, an increasing standard uncertainty with decreasing excitation level is clearly observable.

In addition, the consistency of impedance estimates over the course of the time can be further checked by evaluating vector plots of harmonic impedances. These plots for some of the frequencies are presented in Figs. 10 and 11. Each figure contains 40 estimates of complex impedance values and each value corresponds to 10-s period, over which averaged periodogram was calculated. From the graphs, it can be inferred that variations of impedance estimates are negligible, and the proposed algorithm provides stable values of both resistive and reactive parts.

B. Public Network and Additional Sources of Noise

This part of the experiment involved the same nonlinear load with maximum apparent power of 3 kVA connected at the end of the feeder (household #6) with crest factor set to 2. This provided sufficient excitation level for negative-sequence harmonics. The load was powered by public grid with THD equal to 1.7% with dominating fifth and seventh harmonics. At certain moments of time, two identical solar power inverters were switched on at the households #1 and #2. The slow ramp irradiation profile was applied to solar power emulator, thus providing the same dc input for both inverters. The injected current of only one inverter was measured and 1-cycle rms values of fundamental component are presented in Fig. 12. The combined fundamental current measured at the sending end of the cable is shown in Fig. 13.

It is evident from the presented graphs that solar power inverters introduce some variations into measured current. Moreover, 1-Hz oscillations of fundamental current are clearly visible in the Fig. 12. These oscillations are the result of operation of Maximum Power Point Tracking algorithm implemented in inverters as "perturb and observe."

Furthermore, considerable fluctuations are to be observed at harmonic frequencies for both voltage measured close to the transformer and load current. As an example, Figs. 14 and 15 demonstrate these quantities for 5th- and 11th-harmonic orders, respectively. It can be concluded from the presented graphs that voltage is exposed to deviations due to the influence of background distortion.

Moreover, the operation of solar power inverters contributes to significant variations of harmonic current and dynamic pattern of a dominant nonlinear load can be scarcely distinguished in Fig. 15. The estimates of 5th-harmonic resistance and reactance values based on the proposed methodology are shown

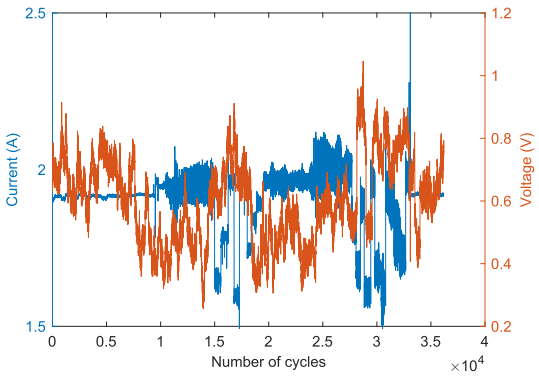

Fig. 14. Fifth-harmonic voltage and current (one-cycle rms).

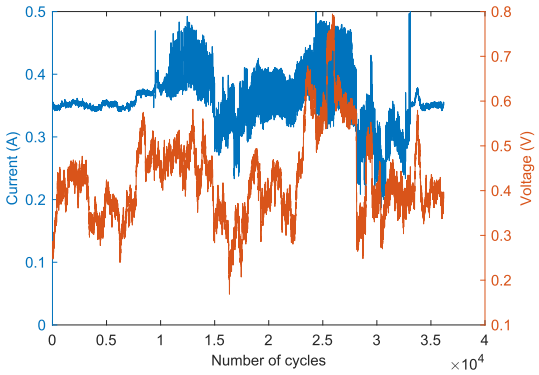

Fig. 15. Eleventh-harmonic voltage and current (one-cycle rms).

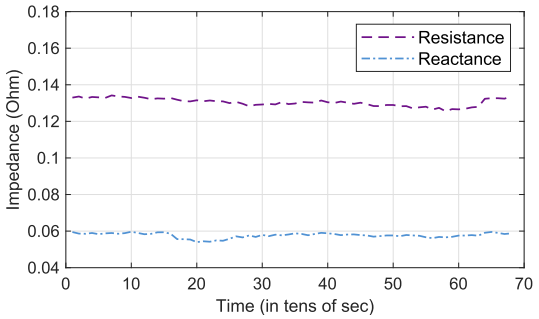

Fig. 16. Fifth-harmonic resistance and reactance values.

in Fig. 16. Clearly, the algorithm provides reasonably stable estimate of both resistive and reactive parts of cable impedance at this harmonic frequency. The calculated difference between extreme points is no more than 10 mΩ for R and X, which indicates that substantial part of the noise introduced by background voltage distortion and solar power was filtered out, whereas the operation of a dominant harmonic source fully contributed to the determination of cable impedance.

At higher harmonic orders characterized by lower current and voltage levels, the influence of noise becomes more pronounced. To evaluate performance of this case, 11th-harmonic resistance and reactance estimates are plotted according to the regime of operation and shown in Figs. 17 and 18. The upper and lower bounds of boxes correspond to 75th percentile and 25th percentile, respectively. Each box is based on

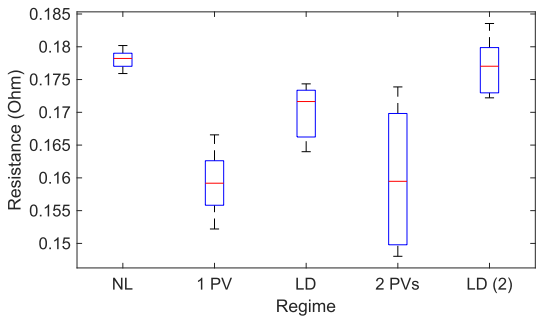

Fig. 17. Resistance at the eleventh harmonic.

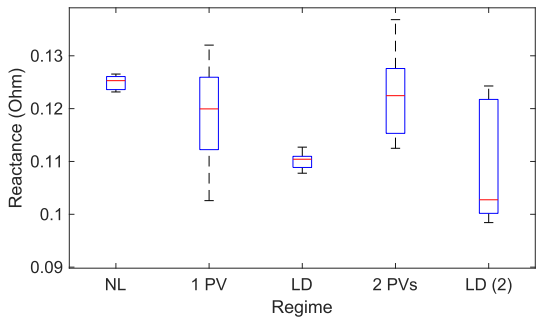

Fig. 18. Reactance at the eleventh harmonic.

100-s observation time. The red lines indicate median values. The following regimes are considered:

1) NL—only nonlinear load operating;
2) 1 PV—first solar inverter switched on;
3) LD—changes in load demand;
4) 2 PVs—second solar inverter switched on and both are now in operation; and
5) LD (2)—changes in load demand.

Refer to Fig. 13 for evaluation of different regimes in time.

From Fig. 17, it can be deduced that operation of PV introduces variation into resistance estimates; however, this variation was decreased during fast changes of load demand indicating that estimate can be improved in noisy environment with low-excitation levels. One of the possible reasons of improvement is the increased correlation between current of dominant harmonic source and its contribution to the voltage distortion.

According to the results, the difference between two extreme median values of resistance estimates is no more than 20 mΩ. Furthermore, Fig. 18 demonstrates that distribution of estimated reactance values did not change significantly during the operation of both PVs in comparison to the 1 PV regime. It is interesting to note that variance of reactance was minimal during LD regime which potentially can indicate the most accurate estimate with median value 0.11043 Ω. In contrast, the largest deviations in reactance values correspond to LD (2). The underlying reason is insufficient excitation of reactive component of the cable during this particular regime of operation. The absolute values of impedance magnitude at 11th harmonic are shown in Fig. 19.

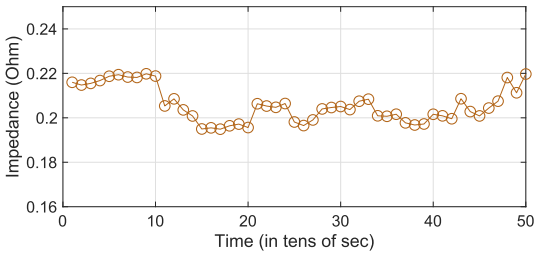

Fig. 19. Magnitudes of the eleventh-harmonic impedance.

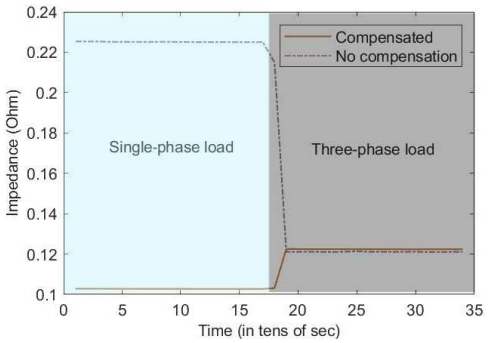

Fig. 20. Fundamental cable impedance estimate for unbalanced and balanced cases.

V. Discussion

A. Considerations on Estimation of Cable Impedance at Fundamental Frequency

In domestic low-voltage distribution system, the vast majority of loads are of a single-phase nature. These loads are connected to different points along the feeder and, in a four-wire system can contribute to a certain extent to neutral current. Thus, depending on the level of current unbalance, an uneven line voltage drop can occur. In theory, it is possible to compensate this effect by employing additional measurement of current in the neutral conductor.

Fig. 20 conveys the idea of phase current compensation by representing estimates of cable impedance. It follows from the graph that impedance becomes slightly overcompensated in comparison with fully balanced regime. One of the possible reasons is the existing leakage from neutral to the ground, which makes actual current reading lower than it is. This implies that in systems where neutral is grounded at each connection point, this effect might become more pronounced.

Another important factor is the size of a neutral conductor, i.e., its ratio to the phase wire. The underlying effect is thoroughly described in [16] by calculating power losses associated with neutral path. Therefore, it is proposed to use cable impedance estimation algorithm only for harmonic frequencies in case when large three-phase nonlinear load produces significant disturbance. It can be inferred from the results of the laboratory experiment that influence of all other small disturbance sources will be filtered out and case can be treated as fully balanced.

Second consideration is the impact of distributed generation connected along the feeder of interest. If part of the fundamental current produced by distributed generation unit is consumed by neighboring load and another part injected to the power grid, then there is no correlation between voltages at sending and receiving end of the cable and load current. Thus, estimation of fundamental cable impedance will give erroneous results. This, however, does not hold for harmonic components, as they tend to propagate from the point of connection of load to the point of common coupling, thus the influence of dominant harmonic source on harmonic voltage distortion at both ends of the cable correlates with the injected harmonic current.

B. Limitations of the Method

As the proposed methodology makes use of single-phase measurements, the strong current unbalance condition will hinder the capability of the algorithm to accurately estimate harmonic line impedance. This can be the case when dominant source of the harmonic disturbance is of a single-phase nature, therefore a fair engineering judgment is important when employing natural variations of such load in practical low-voltage distribution system.

Furthermore, the proposed methodology was developed and tested for systems connected to the secondary winding of transformer configured as "grounded star." It is expected that, in case of transformer's "delta" configuration, no triplen harmonics will flow in the system and consequently no reasonable impedance values for associated frequencies can be obtained.

Moreover, the harmonic excitation level provided by the dominant nonlinear source should be sufficient in order to perform the correct distinction from other sources of the noise. This requirement, however, is dependent on several specific factors, for instance strength of the network and accuracy of the measurement instrumentation. As a general rule, it is recommended to use instruments with superior accuracy levels which are capable of resolving frequency components at frequencies higher than fundamental. Therefore, prior to applying harmonic impedance estimation algorithm all the frequency components with values below the uncertainty level of instrumentation chain must be excluded from the calculation procedure.

C. Applications

Two possible applications are foreseen for the described algorithm. First, it is an online estimation of the harmonic impedance of low-voltage distribution feeders, which is an essential input for further Power Quality assessment procedures. It aims to facilitate the evaluation of emission levels of harmonic producing installations as well as their impact on the voltage quality. Furthermore, knowing accurate harmonic impedances of cables can contribute to determining planning levels of harmonic distortions and setting actual and fair limits.

Second, taking into consideration the concept of estimating correlation between the current of a dominant disturbance source up to the point of its connection and associated harmonic voltage drop, the proposed method can be utilized for physical localization of the harmonic load. The connection point of a dominant harmonic source along the feeder will determine segment of its impedance to be estimated. This segment impedance in turn can be translated to the distance using per km reactance and resistance values for certain cable

type and taking into consideration skin and proximity effect influence.

VI. Conclusion

A novel noninvasive approach for estimating harmonic impedance of low-voltage cable has been proposed. In comparison with existing invasive methods no external excitation source is needed. The described technique can be directly applied to loaded low-voltage feeders, thus allowing to estimate the actual resistance and reactance values during the operation of a cable under the study. The proposed procedure utilizes synchronized two-point measurements which provide an advantage of accurately resolving imaginary part of cable harmonic impedance in presence of fluctuating harmonics.

Only the natural harmonic injections of one dominant nonlinear source are required as an input for the proposed technique. As these injections are typically difficult to fully distinguish from other harmonic producing loads and their impact on voltage, an algorithm aiming to separate the contributions has been developed. This algorithm is based on Welch averaged periodograms, which filters out any uncorrelated signals and increases signal-to-noise-ratio, thus overcoming the deficiency of conventional noninvasive methods.

An output of the developed algorithm is a transfer function which describes the frequency response of LTI system. This transfer function contains real and imaginary components at different frequencies that correspond to harmonic impedance values.

The performance of the method has been tested in laboratory conditions, where a typical low-voltage distribution feeder was set up together with several nonlinear loads connected to it. It was found out that the estimated impedance values are reasonably stable at harmonic frequencies during the three-phase balanced injections of harmonic current. For fifth harmonic, the variation of resistance and reactance estimates was no more than 10 mΩ and for 11th harmonic no more than 20 mΩ. However, the estimate of fundamental frequency impedance might become unreliable under certain circumstances.

The proposed algorithm demonstrated an ability to eliminate possible influence of several connected loads on the final values of cable harmonic impedance. This was achieved by representing their impact as uncorrelated noise in the system and calculating final impulse response based on the injections of dominant harmonic source.

The uncertainty of measurement chain has been evaluated with a conclusion that estimate of impedance magnitude can be improved with the increasing frequency due to better correlation levels between voltage and current. For instance, the standard uncertainty for fundamental impedance was 7.7 mΩ, whereas the calculated value for third harmonic was 3.8 mΩ.

As this method relies mainly on single-phase measurements, a careful consideration should be given to the cases involving strong current unbalance in order to avoid ambiguity of final result.

Finally, the findings presented in this paper provide an opportunity for further research concerned the localization of non-linear loads in distribution systems. This is left for future work.

References

[1] C. H. Chien and R. W. G. Bucknall, "Harmonic calculations of proximity effect on impedance characteristics in subsea power transmission cables," *IEEE Trans. Power Del.*, vol. 24, no. 4, pp. 2150–2158, Oct. 2009.

[2] A. Pagnetti, A. Xemard, F. Paladian, and C. A. Nucci, "An improved method for the calculation of the internal impedances of solid and hollow conductors with the inclusion of proximity effect," *IEEE Trans. Power Del.*, vol. 27, no. 4, pp. 2063–2072, Oct. 2012.

[3] A. J. Urquhart and M. Thomson, "Series impedance of distribution cables with sector-shaped conductors," *IET Gener. Transmiss. Distrib.*, vol. 9, no. 16, pp. 2679–2685, Dec. 2015.

[4] Y. Du and J. Burnett, "Experimental investigation into harmonic impedance of low-voltage cables," *IEE Proc. Gener., Transmiss. Distrib.*, vol. 147, no. 6, pp. 322–328, Nov. 2000.

[5] Z. H. Yuan and Y. Du, "Harmonic impedance of single-core armored cables," in *Proc. IEEE PES Transmiss. Distrib. Conf. Expo.*, vol. 1, Sep. 2003, pp. 45–48.

[6] D. Shi, D. J. Tylavsky, K. M. Koellner, N. Logic, and D. E. Wheeler, "Transmission line parameter identification using PMU measurements," *Eur. Trans. Elect. Power*, vol. 21, no. 4, pp. 1574–1588, 2011.

[7] D. Ritzmann, J. Rens, P. S. Wright, W. Holderbaum, and B. Potter, "A novel approach to noninvasive measurement of overhead line impedance parameters," *IEEE Trans. Instrum. Meas.*, vol. 66, no. 6, pp. 1155–1163, Jun. 2017.

[8] P. Ren, H. Lev-Ari, and A. Abur, "Tracking three-phase untransposed transmission line parameters using synchronized measurements," *IEEE Trans. Power Syst.*, vol. 33, no. 4, pp. 4155–4163, Jul. 2018.

[9] V. Milojević, S. Čalija, G. Rietveld, M. V. Ačanski, and D. Colangelo, "Utilization of PMU measurements for three-phase line parameter estimation in power systems," *IEEE Trans. Instrum. Meas.*, vol. 67, no. 10, pp. 2453–2462, Oct. 2018.

[10] P. A. Pegoraro, K. Brady, P. Castello, C. Muscas, and A. V. Meier, "Line impedance estimation based on synchrophasor measurements for power distribution systems," *IEEE Trans. Instrum. Meas.*, vol. 68, no. 4, pp. 1002–1013, Apr. 2019.

[11] S. Babaev, R. S. Singh, J. Cobben, V. Cuk, and H. Van Den Brom, "Considerations on the performance of multi-point synchronized harmonic measurement system," in *Proc. IEEE 9th Int. Workshop Appl. Meas. Power Syst. (AMPS)*, Sep. 2018, pp. 1–5.

[12] S. Babaev, V. Cuk, J. F. G. Cobben, and H. E. Van Den Brom, "Harmonic source location in the distribution grid using time-synchronized measurements," *Renew. Energy Power Quality J.*, vol. 1, no. 16, pp. 276–280, Apr. 2018.

[13] P. D. Welch, "The use of fast Fourier transform for the estimation of power spectra: A method based on time averaging over short, modified periodograms," *IEEE Trans. Audio Electroacoust.*, vol. AU-15, no. 2, pp. 70–73, Jun. 1967.

[14] D. Borkowski, A. Wetula, and A. Bień, "New method for noninvasive measurement of utility harmonic impedance," in *Proc. IEEE Power Energy Soc. General Meeting*, Jul. 2012, pp. 1–8.

[15] *Evaluation of Measurement Data—Guide to the Expression of Uncertainty in Measurement*, document JCGM 100:2008, 2008.

[16] S. Pajic and A. E. Emanuel, "Effect of neutral path power losses on the apparent power definitions: A preliminary study," *IEEE Trans. Power Del.*, vol. 24, no. 2, pp. 517–523, Apr. 2009.

Stanislav Babaev was born in Russia. He received the M.Sc.(tech.) degree in electrical engineering, with a focus on smart grids, from the Tampere University of Technology, Tampere, Finland, in 2016. He is currently pursuing the Ph.D. degree with the Electrical Energy Systems Group, Eindhoven University of Technology, Eindhoven, The Netherlands.

From 2010 to 2014, he held engineering positions in several energy companies where he was involved in reconstruction and modernization of electrical substations. His current research interests include power quality, power system analysis, and metrology for smart grids.

Sjef Cobben was born in Nuth, The Netherlands. He received the M.Sc.(tech.) and Ph.D. degrees in electrical engineering from the Eindhoven University of Technology, Eindhoven, The Netherlands, in 2002 and 2007, respectively.

He is currently a Research Scientist with Alliander, Arnhem, The Netherlands, specialized in safety of the low-voltage and medium-voltage networks, power quality, and safety of installations connected to the networks. He is also a Part-Time Professor with the Eindhoven University of Technology, Eindhoven, The Netherlands, where he is involved in intelligent grids and power quality. He has authored several books on low-voltage installations and power quality.

Dr. Cobben is a member of several national and international standardization committees about requirements for low- and high-voltage installations and characteristics of the supply voltage.

Vladimir Ćuk received the Dipl.Ing. (M.Sc.) degree in electrical engineering from the School of Electrical Engineering, University of Belgrade, Belgrade, Serbia, in 2005, and the Ph.D. degree from the Electrical Energy Systems Group, Eindhoven University of Technology, Eindhoven, The Netherlands, in 2013.

From 2006 to 2009, he was with the Department of Electrical Measurements, Nikola Tesla Electrical Engineering Institute, Belgrade. He is currently an Assistant Professor with the Eindhoven University of Technology. His current research interest includes electrical power quality.

Helko van den Brom (M'14–SM'15) was born in Utrecht, The Netherlands, in 1971. He received the M.Sc. degree in theoretical solid-state physics from Utrecht University, Utrecht, in 1995, and the Ph.D. degree in experimental solid-state physics from Leiden University, Leiden, The Netherlands, in 2000.

In 2000, he joined Dutch Metrology Institute (VSL), Delft, The Netherlands, where he was involved in the development of Josephson and SET-based electrical quantum standards. He is currently the Principle Scientist, Dutch Metrology Institute (VSL). His current research interests include power quality, high-current transducers, sampling systems, and ac Josephson voltage standards.

Dr. Van den Brom is a member of the Dutch Physical Society (NNV), a Technical Assessor for the Dutch Accreditation Council (RvA), and a Contact Person for VSL in the Technical Committee of Electricity and Magnetism (TCEM) of the European Association of National Metrology Institutes (EURAMET) and its subcommittee of dc and quantum electrical measurements. He was a recipient of the Best Ph.D. Paper Award of the Dutch Journal of Physics (NTvN) in 2000.